Fast Wave Evanescence in Filamentary Boundary Plasmas

J. R. Myra

Lodestar Research Corporation, Boulder, CO, USA

Dec. 2013

submitted to *Physics of Plasmas*

DOE-ER/54392-74 LRC-13-156

LODESTAR RESEARCH CORPORATION

2400 Central Avenue

Boulder, Colorado 80301

Fast Wave Evanescence in Filamentary Boundary Plasmas

J.R. Myra

Lodestar Research Corporation, Boulder, Colorado, USA

Abstract

Radio frequency waves for heating and current drive of plasmas in tokamaks and other magnetic confinement devices must first traverse the scrape-off-layer (SOL) before they can be put to their intended use. The SOL plasma is strongly turbulent and intermittent in space and time. These turbulent properties of the SOL, which are not routinely taken into account in wave propagation codes, can have an important effect on the coupling of waves through an evanescent SOL or edge plasma region. The effective scale length for fast wave (FW) evanescence in the presence of short-scale field-aligned filamentary plasma turbulence is addressed in this paper. It is shown that although the FW wavelength or evanescent scale length is long compared with the dimensions of the turbulence, the FW does not simply average over the turbulent density; rather, the average is over the exponentiation rate. Implications for practical situations are discussed.

PACS: 52.25.Os, 52.35.Ra, 52.50.Qt, 52.55.Fa

I. Introduction

The propagation of plasma waves in the presence of a background of short-scale turbulence has been recognized as an important and scientifically interesting topic for many years. Pioneering theoretical work on this problem was done in the early 1980's [1-3] which resulted in a Fokker-Planck description of the scattering of rays by a random distribution of plane-wave perturbations on the background plasma. This approach was subsequently explored theoretically for a variety of wave regimes (including high-harmonic fast wave, lower hybrid, and electron cyclotron) by other authors.[4-7] Experimental evidence for wave scattering[8-10] including mode conversion induced by scattering[8] was also reported and motivated some of the theoretical work.

Complimentary to the wave-kinetic Fokker-Planck type of approach to theory and modeling, the wave scattering problem has also been considered for the case where the background plasma turbulence contains coherent structures.[11-13] These approaches were partly motivated by theory and observations of the edge and scrape-off-layer (SOL) which showed that the turbulence in those plasmas is dominated by short-scale field-aligned structures often referred to as blob-filaments or simply blobs. Two review articles[14,15] covering theory, experiment and simulation provide addition information and references on this topic. For present purposes we can view a blob as a flux tube containing significantly denser plasma than the surrounding background. Blobs typically have cm scale dimensions perpendicular to the magnetic field B, and much longer scales (several m or more) along B. Relative to the short period ($<< 1\ \mu s$) of rf waves in the ion cyclotron range of frequencies (ICRF) and above, the blob structures are frozen in time, but present a spatially intermittent edge and SOL which the waves must traverse on their way to the core plasma.

In Ref. 11 the scattering of fast and slow waves in the ICRF and lower hybrid frequency regimes was considered. The propagating waves in this study were taken to be incident on an *isolated* cylindrical blob, an assumption which requires a sufficiently large blob separation or equivalently a small blob packing fraction. Calculations were performed analytically by matching the incident plane wave solution onto the interior blob solution and a scattered wave. Scattering widths were derived and the scattered power fraction was estimated using a cold-fluid plasma model. Processes such as scattering-induced mode conversion, scattering resonances, and shadowing were investigated. Subsequently, scattering calculations from an assumed spherical plasma structure using an analogous formalism reported similar results.[13]

The goal of the present paper is to consider a problem much like that described in Ref. 11 but for the case where the incident wave is an evanescent field. In this case, there

is no far-field scattering as such, but the important question becomes one of determining how the effective scale length for evanescence is affected by the presence of the spatially intermittent plasma, i.e. the blob structures.

The practical interest in this problem arises because radio frequency waves meant for heating and current drive in tokamaks and other magnetic confinement devices must first traverse the scrape-off-layer (SOL) before they can be put to their intended use. The turbulent properties of the SOL, which are not routinely taken into account in wave propagation codes, can have an important effect (as we shall see) on the coupling of fast waves through an evanescent SOL or edge plasma region. When the effective scale length for fast wave (FW) evanescence is short compared to the distance between the antenna and the core plasma it is difficult to couple much power into the core. High voltages on the antenna would be required, and this often results in edge power losses and impurity issues,[16-18] and possibly antenna damage from arcing.

The issue of FW coupling through an evanescent SOL may be of particular interest for the ITER tokamak now under construction. The planned ITER FW antenna is located far into the SOL. This has motivated a study by Messiaen and Weynants[19] of FW coupling using a laminar one-dimensional (1D) density profile. These authors found that coupling was very sensitive to the width of the evanescent region below cutoff, and to the profile of the region above cutoff. Slight profile modifications were found to lead to substantial coupling and power capability variations. Given this result, the present study of blob effects (which are a rather extreme profile variation) on evanescence seems well motivated.

This paper here addresses the effective evanescence rate from the perspective of several models. It generalizes to two dimensions (2D) an initial study[12] using a 1D blob lattice model. In Sec. II, the evanescence rate is calculated in a 2D infinite blob lattice using a model wave equation. The main parametric dependencies are deduced from this model. In Sec. III an asymptotic solution is developed for the case where the blobs are sufficiently separated that there are no multiple-blob interactions of the waves. In Sec. IV the formalism of Ref. 11 for the actual fast wave (as opposed to the model wave equation) is applied in the same asymptotic limit of isolated blobs. It is shown that the results for the model wave equation and the fast wave are the same. Finally in Sec. V, the results are summarized and described using an intuitive approach. Practical implications of the work are discussed.

II. 2D blob lattice model

In this section, a model wave equation is solved in the domain of a 2D blob lattice. For the sake of simplicity, a scalar wave model is used here to avoid the full complexities of the fast wave dispersion relation and associated vector polarization. These complexities are treated asymptotically in Sec. IV. The geometry is shown in Fig. 1 which defines the blob radius "a" and the inter-blob spacing (lattice size) parameters L_x and L_y. In this geometry the packing fraction, i.e. the ratio of blob area to area between blobs, is given by

$$f_p = \frac{\pi a^2}{L_x L_y} \tag{1}$$

which can take on values over the range $0 < f_p < \pi/4$ with the upper limit occurring for $L_x = L_y$.

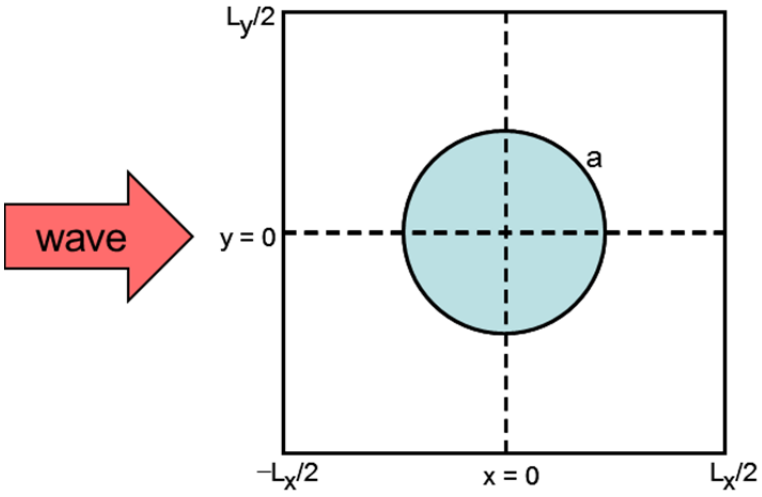

Fig. 1 One cell of a doubly periodic blob lattice. The blob radius is "a"; L_x and L_y specify the blob spacing. The fast wave is incident from the left.

The main physical features of the problem are illustrated here by considering the solution of the following wave problem

$$\nabla^2\Phi = 0\,,\ r < a \tag{2}$$

$$\nabla^2\Phi - \kappa^2\Phi = 0\,,\ r \geq a. \tag{3}$$

where $r = (x^2+y^2)^{1/2}$. This problem models a situation where the blob consists of plasma of sufficient density to be above wave cut-off, so that the waves do not evanesce inside the blob itself. In the vacuum region between the blobs, evanescence occurs at the local

rate κ. As discussed in Sec. V, this situation is the one of most interest for fast wave interactions with turbulent edge and SOL plasmas. Note that we are interested in the case where the (modeled fast wave) wavelength is much larger than the blob dimensions, so propagation characteristics inside the blob are neglected, i.e. ka << 1 where k is the wavenumber in the blob plasma.

The complications in solving Eqs. (2) and (3) are in the associated matching and boundary conditions. At the blob-vacuum interface r = a the wave field and its gradient are continuous

$$\Phi(r = a_-) = \Phi(r = a_+) \tag{4}$$

$$\frac{\partial \Phi}{\partial r}(r = a_-) = \frac{\partial \Phi}{\partial r}\Phi(r = a_+). \tag{5}$$

Periodic solutions are sought in the y-direction

$$\Phi\left(y = \frac{L_y}{2}\right) = \Phi\left(y = -\frac{L_y}{2}\right) \tag{6}$$

$$\Phi_y\left(y = \frac{L_y}{2}\right) = \Phi_y\left(y = -\frac{L_y}{2}\right) \tag{7}$$

where $\Phi_y = \partial\Phi/\partial y$. In the x-direction, the desired solutions are evanescent-periodic, i.e.

$$\Phi\left(x = \frac{L_x}{2}\right) = F\Phi\left(x = -\frac{L_x}{2}\right) \tag{8}$$

$$\Phi_x\left(x = \frac{L_x}{2}\right) = F\Phi_x\left(x = -\frac{L_x}{2}\right) \tag{9}$$

where 0 < F <1 is the sought-after "eigenvalue" to be determined from the solution. Given F, the effective evanescent rate q is then defined by

$$F \equiv e^{-qL} \tag{10}$$

where henceforth $L \equiv L_x = L_y$. The notations L_x and L_y are sometimes retained in the following presentation for pedagogical clarity.

The solution method adopted here is to employ series expansions of the general solution to the wave (Laplace or Helmholtz) equation in the internal (blob) and external (vacuum) regions. The boundary and matching conditions then provide constraints which convert the problem into a generalized eigenvalue matrix problem. The solution method is summarized in an Appendix.

The field pattern for a typical solution is shown in Fig. 2. Note the distortion of the wavefronts by the blob and the more rapid evanescent decay in exterior region. For this case (kL = 4, a/L = 0.25 corresponding to f_p = 0.20) the result is F = 0.0299, q = – *ln* F = 3.51 and hence q/κ = 0.88.

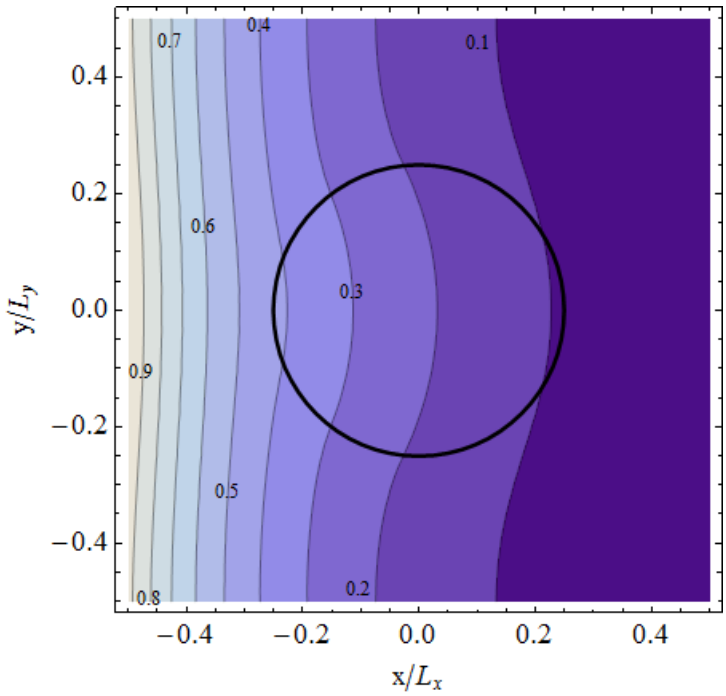

Fig. 2 Field pattern (shaded contours) for |Φ| in the (x, y) plane for the case κL = 4, a/L = 0.25 corresponding to f_p = 0.20. The thick circle is the blob radius r = a and the wave is incident from the left.

It turns out that over a wide parameter range the solutions are conveniently expressed in the parameter space of the packing fraction f_p and the relative evanescence rate q/κ. This result is partly expected from the 1D model investigated in Ref. 12. Figure 3 summarizes the main findings from the 2D blob lattice model. The numerical result for q (normalized to κ) is shown vs. f_p with solid lines for particular values of κL ranging from small to large. For small κL, the results accumulate at a bounding line that is essentially the κL = 0.5 case. The κL << 1, f_p << 1 limit is numerically close to q/κ = 1– f_p/2 moving down and away as f_p increases. For large κL the curves follow q/κ = 1– f_p for f_p << 1 and then move up and away from this line as f_p increases. It will be shown in Sec. III that 1–f_p is the analytical asymptotic limit for large κ and small f_p.

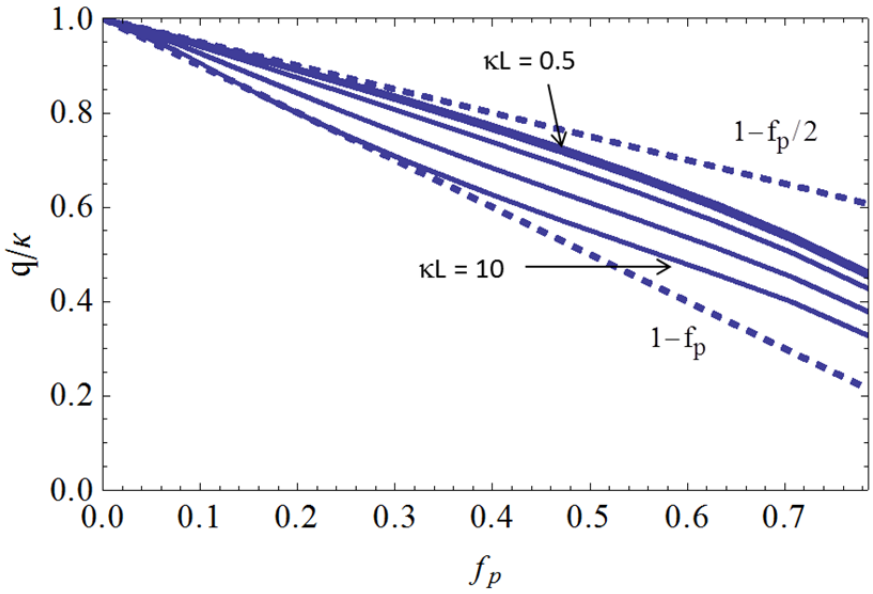

Fig. 3 Relative evanescence rate from the 2D blob lattice model. Numerical results for κL = 0.5, 1, 2, 4, 7, 10 are shown with solid lines. The dashed lines are analytical scalings that bound the results.

An important result from Fig. 3 is the all the cases are bounded by the dashed lines i.e.

$$1-f_p < q/\kappa < 1-f_p/2\,. \tag{11}$$

This has the advantage that it makes numerical work unnecessary for rough estimates, and, as discussed in the Sec. V, it enables an intuitive interpretation of the results.

III. Asymptotic solution of the model problem

In this section the solution of the model problem of Sec. II is derived in the asymptotic limit of large $\kappa L >> 1$. In this limit, the coupling between adjacent cells in the lattice is negligible and we can treat the interaction of an evanescent field with a single isolated blob. The basic method is the same as described in Ref. 11, using scattering theory, but with modifications to account for the evanescence of the fields and the scalar nature of the model described in Sec. II.

The incident field in the exterior region is

$$\Phi^{(i)} = e^{ik_x x} = e^{-\kappa x} = \exp(-\kappa r\cos\theta) \tag{12}$$

where $x = r\cos\theta$, $k_x = i\kappa$ and we take the incident $k_y = 0$. Using Bessel identities we have

$$\Phi^{(i)} = \sum_m (-)^m I_m(\kappa r)\, e^{im\theta} . \tag{13}$$

The "scattered wave" (actually an evanescent field) is written as

$$\Phi^{(s)} = \sum_m \Phi_m^{(s)} K_m(\kappa r)\, e^{im\theta} \tag{14}$$

where K_m is the decaying Bessel function as r gets large. The interior (blob) solution is

$$\Phi^{(b)} = \sum_m \Phi_m^{(b)} e^{im\theta} \left(\frac{r}{a}\right)^m . \tag{15}$$

Applying the matching conditions at r = a and eliminating $\Phi_m^{(b)}$ results in

$$\Phi_m^{(s)} = \frac{(-)^{m+1}\left(mI_m - zI'_m\right)}{\left(mK_m - zK'_m\right)} \tag{16}$$

where all Bessel functions are evaluated at z = κa. The total exterior wave solution is then given by $\Phi \equiv \Phi^{(i)} + \Phi^{(s)}$.

To calculate the evanescence rate for large κr we take the asymptotic limit of the Bessel functions for κr >> m

$$K_m(\kappa r) \sim \left(\frac{\pi}{2\kappa r}\right)^{1/2} e^{-\kappa r} \tag{17}$$

For large κr the scattering term $\Phi^{(s)}$ is small compared with the incident field $\Phi^{(i)}$ by the factor $1/(\kappa r)^{1/2}$ and henceforth is treated as a perturbation. Thus to leading order in the scattering

$$\left|\Phi\right|^2 = e^{-2\kappa x} + 2e^{-\kappa x}\, \mathrm{Re}\,\Phi^{(s)} . \tag{18}$$

Next the evanescence factor is defined as

$$F = \frac{\left\langle \left|\Phi(x = L_x/2)\right|^2 \right\rangle_y^{1/2}}{\left\langle \left|\Phi(x = -L_x/2)\right|^2 \right\rangle_y^{1/2}} \tag{19}$$

where $\langle \ldots \rangle_y$ is a y-average. After some algebra one obtains

$$F = e^{-\kappa L_x}\left[1 + e^{\kappa L_x/2}\, \mathrm{Re}\left\langle \Phi^{(s)}(L_x/2)\right\rangle_y - e^{-\kappa L_x/2}\, \mathrm{Re}\left\langle \Phi^{(s)}(-L_x/2)\right\rangle_y\right] \tag{20}$$

where

$$\mathrm{Re}\left\langle \Phi^{(s)}(x)\right\rangle = \left(\frac{\pi}{2}\right)^{1/2} \frac{1}{\kappa L_y}\, \mathrm{Re} \sum_m \Phi_m^{(s)} \int_{-\infty}^{\infty} d\hat{y}\ \frac{\exp[-(\hat{x}^2 + \hat{y}^2)^{1/2} + im\theta]}{(\hat{x}^2 + \hat{y}^2)^{1/4}} \tag{21}$$

Here $\kappa x = \hat{x}$, $\kappa y = \hat{y}$, $\tan\theta = \hat{y}/\hat{x}$, $\kappa r = (\hat{x}^2 + \hat{y}^2)^{1/2}$ and the y-integration has been extended to the infinite domain, valid for the leading asymptotic result.

To make further analytical progress it is necessary to invoke the $z \equiv \kappa a << 1$ expansions of $\Phi_m^{(s)}$. Note that $\kappa a << 1$ and $\kappa L >> 1$ together imply that $f_p << 1$. It is readily shown that

$$\Phi_0^{(s)} = \frac{z^2}{2} + ... \tag{22}$$

$$\Phi_{-1}^{(s)} = \frac{1}{\gamma_E - \ln 2 + \ln z} + \frac{z^2}{4(\gamma_E - \ln 2 + \ln z)^2} + ... \tag{23}$$

$$\Phi_{-2}^{(s)} = \frac{z^2}{2} + ... \tag{24}$$

and all other terms are higher order than z^2. Here γ_E is Euler's constant.

The leading term in the z expansion therefore comes from m = –1. However, after some further calculations, it can be shown that the resulting m = –1 contribution to F vanishes for large $\zeta \equiv \kappa L_x/2$. Thus, the desired asymptotic $\zeta >> 1$ result comes from the z^2 terms in $\Phi_m^{(s)}$ for m = 0 and m = –2. For m = 0 one finds

$$\mathrm{Re}\left\langle \Phi_0^{(s)}(x) \right\rangle = \left(\frac{\pi}{2}\right)^{1/2} \frac{\kappa a^2}{2L_y} \int_{-\infty}^{\infty} d\hat{y} \; \frac{\exp[-(\hat{x}^2 + \hat{y}^2)^{1/2}]}{(\hat{x}^2 + \hat{y}^2)^{1/4}} \sim \frac{\pi\kappa a^2}{2L_y} e^{-\kappa|x|} \tag{25}$$

where the final form is the large $\hat{x}$ asymptotic limit. Similarly, for m = –2 one has

$$\mathrm{Re}\left\langle \Phi_{-2}^{(s)}(x) \right\rangle = \left(\frac{\pi}{2}\right)^{1/2} \frac{\kappa a^2}{2L_y} \int_{-\infty}^{\infty} d\hat{y} \; \frac{(\hat{x}^2 - \hat{y}^2)\exp[-(\hat{x}^2 + \hat{y}^2)^{1/2}]}{(\hat{x}^2 + \hat{y}^2)^{5/4}} \sim \frac{\pi\kappa a^2}{2L_y} e^{-\kappa|x|} \tag{26}$$

where $\hat{r}^2 \cos 2\theta = \hat{r}^2 \cos^2\theta - \hat{r}^2 \sin^2\theta = \hat{x}^2 - \hat{y}^2$ has been used. Substituting these contributions into Eq. (20) yields

$$F = e^{-\kappa L_x}\left(1 + \frac{\pi\kappa a^2}{L_y}\right) = e^{-\kappa L_x}\left(1 + \kappa L_x f_p\right) \tag{27}$$

which gives the normalized decay rate

$$\frac{q}{\kappa} \equiv -\frac{\ln F}{\kappa L_x} = 1 - f_p \tag{28}$$

provided $\kappa L_x f_p << 1$ to expand the logarithm (otherwise the treatment of the scattered field as a perturbation breaks down). This result is in agreement with the numerical results in Fig. 3 and will also turn out to be identical to the asymptotic result for the FW case.

IV. Asymptotic solution of the fast wave problem

Up until now in the paper, consideration of the evanescence problem has been restricted to the case of the Helmholtz-Laplace model given by Eqs. (2) and (3). It is important to gain some insight into how faithfully this model reproduces the actual FW behavior. In this section the solution of the full FW problem is derived in the asymptotic limit of large $\kappa L >> 1$. As in Sec. III, we can treat the interaction of an evanescent field with a single isolated blob, and the formalism again closely follows Ref. 11. The derivation, which is tedious but straightforward, will only be summarized here. The notation for the most part follows Ref. 11, which the reader is referred to for details.

The basic FW equation set is given by Eqs. (MD-2) and (MD-3) where the MD prefix indicates equation numbers from Ref. 11. The general solution may still be written in the form given by Eq. (MD-6), namely

$$\mathbf{E} = \sum_{m,j} e^{im\theta} E_m^{(j)} \mathbf{W}_m^{(j)}(r) \tag{29}$$

where the quantities $\mathbf{W}_m^{(j)}(r)$ consist of combinations of Bessel functions. Here j is an index which enumerates the incident, internal and scattered wave fields and $E_m^{(j)}$ are the unknown coefficients to be solved for. The calculations go through if we continue the Bessel functions into the complex plane, effectively making the change

$$i^m J_m(k_\perp r) \to (-)^m I_m(\kappa r) \tag{30}$$

where $k_\perp = i\kappa$ for the evanescent waves. Taking the limit $k_\perp a << 1$ as in Ref. 11 for the wave-fields both internal and external to the blob, one arrives, as before, as Eq. (MD-31) giving the ratio of the scattered solution $E^{(1)}$ to the incident wave $E^{(0)}$ as

$$\begin{aligned}\frac{E^{(1)}}{E^{(0)}} = &-\frac{i\pi\xi^2}{4}\frac{(Q_{bi}-1)\xi^2-(Q_i-1)\xi_b^2}{(Q_{bi}-1)\xi^2-(Q_i+1)\xi_b^2}\delta_{m,1} \\ &-\frac{i\pi\xi^2}{4}\frac{(Q_{bi}+1)\xi^2-(Q_i+1)\xi_b^2}{(Q_{bi}+1)\xi^2-(Q_i-1)\xi_b^2}\delta_{m,-1}\end{aligned} \tag{31}$$

where $\xi = k_\perp a$, $\xi_b = k_{\perp b} a$ and subscript b indicates evaluation using plasma parameters inside the blob. Here $Q = i\varepsilon_\times/(\varepsilon_\perp - n_\parallel^2)$ and $Q_i = \mathrm{Im}\, Q$ where $\varepsilon_\times$ and $\varepsilon_\perp$ are the usual cold fluid components of the dielectric tensor and $n_\parallel = k_\parallel c/\omega$.

From this point on, the calculations start to depart from Ref. 11 since the present calculation investigates different limits and different outputs (namely the evanescence

factor F rather than the far-field scattering width). The simplest limit is $\xi << 1$, and $\xi_b = 0$ which also corresponds to the limit considered for the model problem. In this case

$$\frac{E^{(1)}}{E^{(0)}} = -\frac{i\pi\xi^2}{4}(\delta_{m,1} + \delta_{m,-1}) \tag{32}$$

The total external solution consists of the incident wave and the decaying m = ±1 Hankel functions embedded in $\mathbf{W}_m^{(j)}(r)$. In the asymptotic limit $\kappa r >> 1$, the H_m' terms are dominant in the scattered solution. After some algebra using the explicit forms for $\mathbf{W}_m^{(j)}(r)$ given in Appendix D of Ref. 11, one obtains the total field to first order in the scattered solution as

$$E_y = e^{-\kappa x} + \frac{(2\pi)^{1/2}}{2}\kappa^2 a_b^2 \frac{e^{-\kappa r}}{\sqrt{\kappa r}}\cos\theta(iQ_i \sin\theta + \cos\theta). \tag{33}$$

Here the $\cos\theta$ factor arises from the m = ±1 contributions to the scattering and the (Q sin θ + cos θ) factor arises from the identity[11] $E_y^{(1)} = E_\theta^{(1)}(Q\sin\theta + \cos\theta)$.

Continuing to retain only first order contributions from the scattered field,

$$\left\langle \left|E_y\right|^2 \right\rangle_y = e^{-2\kappa x} + (2\pi)^{1/2} e^{-\kappa x} \frac{\kappa^3 a^2 x^2}{L_y} f_1(\hat{x}). \tag{34}$$

where

$$f_1(\hat{x}) = \int_{-\infty}^{\infty} d\hat{y} \frac{e^{-\sqrt{\hat{x}^2 + \hat{y}^2}}}{(\hat{x}^2 + \hat{y}^2)^{5/4}} \tag{35}$$

$\hat{x} = \kappa x$, $\hat{y} = \kappa y$ and the integration limits have be extended to infinity using $\kappa L_y >> 1$. Using the definition of F given in Eq. (19) with Φ now replaced by E_y, the evanescence factor is

$$F = e^{-\kappa L_x}\left[1 + (2\pi)^{1/2}\frac{\kappa^3 a^2 L_x^2}{4L_y} f_1(\zeta)\sinh(\zeta)\right] \tag{36}$$

where $\zeta = \kappa L_x/2$. Thus the normalized decay rate is

$$\frac{q}{\kappa} = 1 - f_p g(\zeta) \tag{37}$$

where

$$g(\zeta) = \frac{2}{(2\pi)^{1/2}}\zeta^2 \sinh(\zeta) f_1(\zeta) \tag{38}$$

and only the leading the leading asymptotic terms in $\zeta >> 1$ are significant. It can be shown that $g(\zeta) \sim 1$ for $\zeta \to \infty$. This completes the demonstration that Eqs. (38) and (27)

are equivalent asymptotically, i.e. the model Helmholtz problem and the full FW problem give the same result for the dependence of the normalized evanescence rate on the packing fraction in the limit $\kappa L >> 1$.

V. Discussion and conclusions

When expressed in terms of the packing fraction, the results of this paper are very similar to those of a simple 1D model.[12] In that model, for $\kappa L >> 1$ but f_p arbitrary, the leading order result was

$$\frac{q}{\kappa} = 1 - f_p \tag{39}$$

while for $f_p << 1$ and $\kappa L \sim 1$ the leading order result was

$$\frac{q}{\kappa} = 1 - \frac{1}{2} f_p \tag{40}$$

Interestingly, Eq. (40) is the same upper bound shown in the numerical results of Fig. 3.

These 1D results have an intuitive heuristic interpretation. Consider the net decay of the fields over a length $L = L_1 + L_2$ where L_1 and L_2 represent regions with corresponding evanescent decay rates q_1 and q_2. Let

$$q = \frac{q_1 L_1 + q_2 L_2}{L} \tag{41}$$

In the case $q_2 = 0$ (e.g. representing the high density blob where the FW propagates) then one obtains $q = q_1(1 - f_p)$ recovering previous results. Thus we conclude that the evanescent wave fields effectively average over the local exponentiation rate. In practical FW coupling calculations, this can be very different from calculating the exponentiation rate using an average density.

To examine the implications of this, consider the specific application to FW propagation in a typical SOL plasma. The FW dispersion relation is

$$n_\perp^2 = \frac{(\varepsilon_\perp - n_\parallel^2 - \varepsilon_\times)(\varepsilon_\perp - n_\parallel^2 + \varepsilon_\times)}{(\varepsilon_\perp - n_\parallel^2)} \tag{42}$$

At very low densities with respect to cutoff we have evanescence with

$$n_\perp^2 \to 1 - n_\parallel^2 \approx -n_\parallel^2 \tag{43}$$

At high densities, well above cutoff, noting that $|\varepsilon_\times| > |\varepsilon_\perp|$, $\varepsilon_\times > 0$, $\varepsilon_\perp < 0$, we have propagation with

$$n_{\perp}^2 = \frac{(\varepsilon_{\perp} - \varepsilon_{\times})(\varepsilon_{\perp} + \varepsilon_{\times})}{\varepsilon_{\perp}} = C_{\varepsilon} n_e \qquad (44)$$

where C_ε is a positive constant. Thus, if the blobs and holes (spaces between blobs) are both at very low density, the evanescence rate is independent of density, and spatial intermittency will have no effect. On the other hand, if the blobs are above cutoff, and the holes below cutoff, the spatial intermittency of the blob-filaments will have an important effect. In this case, averaging the evanescence rate (not the density) is the correct approach.

As mentioned in the introduction, FW coupling through an evanescent and turbulent SOL may be of particular interest for ITER. The present work suggests that calculated evanescence rates based on an average 1D radial density profile may be overly optimistic. From a modeling viewpoint this motivates the inclusion of spatial intermittency of the plasma profiles in FW propagation and coupling codes. From an experimental and design point of view, it may support techniques such as gas injection[20] to better control the SOL density profile and hence mitigate rapid evanescence and its detrimental effect on FW coupling.

In conclusion, although the FW wavelength (evanescent scale length) in the tokamak SOL is typically long compared with the dimensions of the filamentary turbulence, the FW does not simply average over the turbulent density. Rather, the average is over the exponentiation rate (inverse decay length); thus the evanescence is usually controlled by the density between blobs-filaments where the exponentiation rate is fastest. Some features of this problem may be generic for waves propagating through short scale structures. It was found that 2D asymptotic solutions of a model Helmholtz problem and the more complicated FW problem can be described by a general result; which also incorporates 1D results from a very simple model.

Acknowledgments

Discussions with the rf SciDAC team (Center for Simulation of Wave-Plasma Interactions) and in particular with Dan D'Ippolito are gratefully acknowledged. This work was supported by the U.S. Department of Energy (DOE) under grant DE-FG02-97ER54392; however, such support does not constitute an endorsement by the DOE of the views expressed herein.

Appendix: Solution method for the blob lattice problem

In this appendix it is shown how the problem defined by Eqs. (2) – (9) is solved numerically by expressing it as a generalized eigenvalue problem.

In the interior region, the solution is expanded in polar coordinates

$$\Phi = \sum_{m=0}^{N-1} C_m \cos(m\theta)\left(\frac{r}{a}\right)^m, \quad r < a \tag{A1}$$

where up-down symmetry is explicitly invoked. In the exterior region the evanescent solution is expanded in terms of Bessel functions

$$\Phi = \sum_{m=0}^{N-1} \cos(m\theta)[A_m I_m(\kappa r) + B_m K_m(\kappa r)], \quad r > a \tag{A2}$$

The two matching conditions at r = a are then used to eliminate B_m and C_m in terms of A_m. For the periodic and evanescent-periodic boundary conditions on the edges of the box, an error minimization procedure is employed. The function to be minimized is defined as

$$W = W_1 + W_2 + W_3 \tag{A3}$$

where

$$W_1 = \int_{-L_x/2}^{L_x/2} dx\, \Phi_y\left(y = \frac{L_y}{2}\right)^2 \tag{A4}$$

$$W_2 = \int_{-L_y/2}^{L_y/2} dy \left[\Phi\left(x = \frac{L_x}{2}\right) - F\Phi\left(x = -\frac{L_x}{2}\right)\right]^2 \tag{A5}$$

$$W_3 = \int_{-L_y/2}^{L_y/2} dy \left[\Phi_x\left(x = \frac{L_x}{2}\right) - F\Phi_x\left(x = -\frac{L_x}{2}\right)\right]^2 \tag{A6}$$

Converting between the (x,y) coordinates in W and the (r, θ) coordinates in the fundamental expansions of Eqs. (A1) and (A2) then results in an expression for W in terms of the A_m,

$$W = \sum_{km} A_k A_m \left(R_{km}^{(0)} + FR_{km}^{(1)} + F^2 R_{km}^{(2)}\right) \tag{A7}$$

The matrix elements $R_{km}^{(j)}$ have explicit but lengthy expressions that are conveniently coded using the symbolic algebra capabilities of the *Mathematica* language. An example contribution to a matrix element is

$$\Lambda^{(a)}_{km} = \int dy\, G_{k+} G_{m+} \tag{A8}$$

where the integral extends over the side of the box,

$$G_m(r,\theta) = \cos(m\theta)\left[\left(\frac{r}{a}\right)^m - \left(\frac{a}{r}\right)^m\right] \tag{A9}$$

and the + and – subscripts indicate evaluation at fixed x = $\pm L_x/2$. Importantly, the matrices $R^{(j)}_{km}$ are symmetric.

The next step is to minimize W with respect to the A_m. Taking account of the symmetry of the matrices, the condition for a minimum of W is

$$\frac{\partial W}{\partial A_n} = 2\sum_{km}\left(R^{(0)}_{nm} + FR^{(1)}_{nm} + F^2 R^{(2)}_{nm}\right)A_m = 0 \tag{A10}$$

which gives a null-space problem with free parameter F. This is not quite yet in the form of a standard eigenvalue problem because F appears quadratically. Suppressing the matrix indices, and writing superscripts (0), (1), (2) as subscripts for notational brevity, the equation is

$$(R_0 + FR_1 + F^2 R_2)\cdot A = 0 \tag{A11}$$

Let

$$B = FR_2 \cdot A \tag{A12}$$

to obtain

$$(R_0 + FR_1)\cdot A + FB = 0 \tag{A13}$$

This can be written in the enlarged space of (A,B) as the block matrix problem

$$\begin{pmatrix} R_0 & 0 \\ 0 & 1 \end{pmatrix}\cdot\begin{pmatrix} A \\ B \end{pmatrix} = F\begin{pmatrix} -R_1 & -1 \\ R_2 & 0 \end{pmatrix}\cdot\begin{pmatrix} A \\ B \end{pmatrix} \tag{A14}$$

which is a generalized eigenvalue problem that can be solved by standard numerical packages.

References

1 P. T. Bonoli and E. Ott, Phys. Rev. Lett. **46**, 424 (1981); and E. Ott, Phys. Fluids **22**, 1732 (1979).

2 M. Ono, Phys. Fluids **25**, 990 (1982).

3 P. L. Andrews and F. W. Perkins, Phys. Fluids **26**, 2537 (1983).

4 K. Hizanidis, A. K. Ram, Y. Kominis, and C. Tsironis, Phys. Plasmas **17**, 022505 (2010).

5 C. Tsironis, A. G. Peeters, H. Isliker, D. Strintzi, I. Chatziantonaki, and L. Vlahos, Phys. Plasmas **16**, 112510 (2009).

[6] T. K. Mau, B. P. LeBlanc, J. E. Menard, M. Ono, C. K. Phillips, and J. R. Wilson, AIP Conf. Proc. (American Inst. Phys., Melville, 2001), Vol. 595, p. 170.
[7] M. Ono, J. Hosea, B. LeBlanc, J. Menard, C.K Phillips, R. Wilson, P. Ryan, D. Swain, J. Wilgen, S. Kubota and T.K. Mau, AIP Conf. Proc. (American Inst. Phys., Melville, 2001), Vol. 595, p. 162.
[8] R.I. Pinsker, Fast Wave Current Drive Experiments on the Princeton Large Torus, Ph. D dissertation, Princeton University (1988).
[9] J. D. Moody, M. Porkolab, C. L. Fiore, F. S. McDermott, Y. Takase, J. Terry, and S. M. Wolfe, Phys. Rev. Lett. **60**, 298 (1988).
[10] V. Pericoli-Ridolfini, L. Giannone, and R. Bartiromo, Nucl. Fusion **34**, 469 (1994).
[11] J. R. Myra and D. A. D'Ippolito, Phys. Plasmas **17**, 102510 (2010).
[12] J.R. Myra and D.A. D'Ippolito, AIP Conf. Proceedings (American Inst. Phys., Melville, 2011) Vol. 1406, p. 219.
[13] A. K. Ram, K. Hizanidis, and Y. Kominis, Phys. Plasmas **20**, 056110 (2013).
[14] S. I. Krasheninnikov, D. A. D'Ippolito, and J. R. Myra, J. Plasma Physics **74**, 679 (2008).
[15] D.A. D'Ippolito, J.R. Myra and S.J. Zweben, Phys. Plasmas **18**, 060501 (2011).
[16] J.-M. Noterdaeme and G. Van Oost, Plasma Phys. Control. Fusion **35**, 1481 (1993).
[17] M. Ono, Phys. Fluids B **5**, 241 (1993).
[18] J. R. Myra, D. A. D'Ippolito, D.A. Russell, L. A. Berry, E. F. Jaeger and M. D. Carter, Nucl. Fusion **46**, S455 (2006).
[19] A. Messiaen and R. Weynants, Plasma Phys. Control. Fusion **53**, 085020 (2011).
[20] P. Jacquet, V. Bobkov, M.-L. Mayoral, I. Monakhov,J.M. Noterdaeme, A. Scarabosio, I. Stepanov, M. Vrancken, E.Wolfrum and the ASDEX Upgrade Team, Nucl. Fusion **52**, 042002 (2012).